5-2010

Velocity distribution of dark Matter halos: A critical test for the Λ cold dark matter model

Robert Jo Thompson
University of Nevada Las Vegas

VELOCITY DISTRIBUTION OF DARK MATTER HALOS: A CRITICAL TEST FOR THE Λ COLD DARK MATTER MODEL

by

Robert Jo Thompson

Bachelor of Science
University of Nevada Las Vegas
2008

A thesis submitted in partial fulfillment
of the requirements for the

Master of Science Degree in Astronomy
Department of Astronomy
College of Sciences

Graduate College
University of Nevada, Las Vegas
May 2010

UNLV
UNIVERSITY OF NEVADA LAS VEGAS

THE GRADUATE COLLEGE

We recommend the thesis prepared under our supervision by

Robert Jo Thompson

entitled

Velocity Distribution of Dark Matter Halos: a Critical Test for the Λ Cold Dark Matter Model

be accepted in partial fulfillment of the requirements for the degree of

Master of Science in Astronomy
Physics and Astronomy

Kentaro Nagamine, Committee Chair

Daniel Proga, Committee Member

George Rhee, Committee Member

Balakrishnan Naduvalath, Graduate Faculty Representative

Ronald Smith, Ph. D., Vice President for Research and Graduate Studies
and Dean of the Graduate College

May 2010

ABSTRACT

Velocity Distribution of Dark Matter Halos: a Critical Test for the Λ Cold Dark Matter Model

by

Robert Jo Thompson

Dr. Kentaro Nagamine, Examination Committee Chair
Professor of Astronomy
University of Nevada, Las Vegas

The existence of a bullet cluster (such as 1E0657-56) poses a challenge to the concordance Λ cold dark matter model. Here we investigate the velocity distribution of dark matter halo pairs in large N-body simulations with differing box sizes and resolutions. We examine various basic statistics such as halo masses, relative halo velocities, collisional angles, and separation distances in our simulations. We then compare the results to the observational properties of 1E0657-56. Our results suggest that it is very difficult to produce such a halo pair with such a high relative velocity at a redshift of z=0. The relative velocities increase at higher redshift, and we find several candidate pairs in a volume of $(2\ h^{-1}\mathrm{Gpc})^3$ at the same redshift as 1E0657-56, z=0.296. However, most of these candidate pairs are separated by too large of a distance.

TABLE OF CONTENTS

LIST OF FIGURES

ACKNOWLEDGMENTS

I would first like to thank Dr. Kentaro Nagamine for welcoming me into his office just over two years ago, and introducing me to the world of computational astrophysics. Your constant encouragement has nourished my passion for astronomy, and your amazing work ethic inspires me to be a better astronomer. Thank you for your guidance and patience. Next I would like to thank Dr. Lon Spight for teaching me to always be skeptical, it plays an important role in my everyday life. I would like to acknowledge Dr. Proga, Dr. Nagamine, Dr. Lepp, Dr. Rhee, and Dr. Zhang for teaching amazingly insightful graduate courses over the past two years. You have all made a great impact on my understanding of your respective subjects. Thanks to Jun-Hwan Choi for always being available and willing to help. I look forward to our future collaborations. Thanks to the many graduate students who have provided stimulating conversation and encouragement. John Kilburg, I appreciate your high level of tolerance and patience. Especially when I do things like crash Sirius, I won't let it happen again. I would like to thank Dr. Victor Kwong for believing in me and giving me a chance in the graduate program. Finally, I would like to thank my friends and family for their love and support.

CHAPTER 1

INTRODUCTION

Dark Matter

A Swiss astronomer by the name of Fritz Zwicky was the first to infer the existence of dark matter (DM) in 1933. He was using the virial theorem to calculate the total mass of the Coma cluster, and found that it was $\simeq$166 times more massive than one would expect from luminosity measurements (Zwicky, 1937). Unfortunately his ideas were not immediately embraced.

Theorists also found themselves with a need for this missing matter. Ostriker & Peebles (1973) studied the stability of flattened galaxies in numerical simulations and found that galaxies with an added spherical (halo) component were more stable. Galaxies without the halo experienced a violent instability that could not be related to any peculiarities of the model. It was their conclusion that the halo masses exterior to the observed disks may be extremely large.

Up until this point in history there was little conclusive findings that an unseen matter existed. The first clear observational evidence for dark matter came from Rubin et al. (1980) detailing the group's work on galaxy rotation curves. Rotation curves measure the rotational velocity of gas and stars as a function of their distance from the center of the galaxy. It is expected from Newton's laws of gravity that the farther from the center a star is, the slower its rotational velocity. Rubin and her collaborators observed that the velocities were actually slowly rising in most galaxies even out to the farthest measured point. These observations led Rubin and her team to the conclusion that the 21 spiral galaxies they studied all must have a significant mass located beyond the optical image.

Many dark matter theories came about in the early 1980s. The three most prominent ones that employed non-baryonic matter are called 'hot', 'warm', or 'cold' dark

matter, and they interact only through gravity, not through the electromagnetic force. The hot dark matter theory describes particles traveling at ultra-relativistic velocities, and predicts that the structure forms through fragmentation. This is known as the 'top-down' scenario wherein large superclusters form early on and fragment into smaller pieces such as the Milky Way. The cold dark matter (CDM) model suggests that the particles move with slower velocities, and that the structure forms hierarchically. This scenario is known as 'bottom-up', where smaller structures form first and then merge to create larger structures (Blumenthal et al., 1984). Then there is warm dark matter, which is a mixture of both hot and cold dark matter. The cold dark matter theory quickly became the leading candidate due to it's ability to reproduce large scale structures resembling observations through the use of simulations (Davis et al., 1985).

ΛCDM Model

Currently the most widely accepted model for the history of our universe is referred to as the ΛCDM model. It is based on the cosmological principle which states that the universe is spatially homogenous and isotropic, which is empirically justified on scales larger than ∼100 Mpc. A solution to the Einstein field equations of General Relativity describing such a universe was found by Friedmann (1922, 1924), and independently by Lemaître (1927). Later through the work of Howard P. Robertson and Arthur G. Walker, these solutions were proved to be the only solutions to describe a space-time that was spatially homogenous and isotropic (Robertson, 1935, 1936a,b; Walker, 1937). This solution came to be known as the Friedmann-Lemaître-Robertson-Walker (FLRW) metric.

By writing the Einstein field equations for the FLRW metric, Friedmann derived his first equation:

$$H^2 = \left(\frac{\dot{a}}{a}\right)^2 = \frac{8\pi G}{3}\rho - \frac{kc^2}{a^2} + \frac{\Lambda c^2}{3}, \tag{1.1}$$

which is just a simple reduced form of the Einstein equation. Here H is the Hubble constant; a is the scale factor of the universe, which is related to the cosmological redshift by

$$\frac{1}{a} \equiv 1 + z; \tag{1.2}$$

G represents Newton's gravitational constant (G=6.67$\times$10^{-8} cm^{3}g^{-1}s^{-2}); ρ is the mass density of the universe composed of both baryonic and non-baryonic dark matter; k is the spatial curvature which takes the form of three solutions (k=0 for a flat universe, k=-1 for a negatively curved or closed universe, and k=+1 for a positively curved or open universe); and Λ is the cosmological constant that represents the vacuum energy. This parameter allows for the current accelerating expansion of the universe and can also be represented as the fractional energy attributed to the vacuum energy Ω_Λ.

If we assume the cosmological constant Λ & the spatial curvature k are equal to zero, we can solve Equation (1.1) for a critical density in which the universe remains flat:

$$\rho_{c,0} = \frac{3H_0^2}{8\pi G} = 2.77 \times 10^{11}\ h^2 M_\odot \mathrm{Mpc}^{-3}. \tag{1.3}$$

Due to constant improvements in technology, and hence measurements of H_0, we leave these equations in terms of the Hubble constant where $h \equiv H_0/100\,\mathrm{km\,s^{-1}\,Mpc^{-1}}$. We then define the ratio of current matter density to the critical matter density as

$$\Omega_\mathrm{m} \equiv \frac{\rho_m}{\rho_c}. \tag{1.4}$$

The values of Ω_Λ, Ω_m, & H_0 are well constrained by supernova type Ia data (Kowalski et al., 2008) and measurements of the anisotropies in the cosmic microwave background (CMB; Komatsu et al., 2009, 2010).

Motivation for Current Work

The observations of the massive cluster of galaxies 1E0657-56 suggest a much higher relative dark matter halo velocity than one would expect by the ΛCDM model. This system includes a massive sub-cluster (the bullet) with $M_{\rm bullet}\simeq 1.5\ \times 10^{14} M_{\odot}$ that has fallen through the parent cluster of $M_{\rm parent}\simeq 1.5\ \times 10^{15} M_{\odot}$ roughly 150 million years ago and is observed to be separated by an approximate distance of $\simeq 0.72$Mpc (Clowe et al., 2004, 2006; Bradač et al., 2006). The above masses were determined by weak and strong gravitational lensing studies. The uniqueness of this system comes from the collision trajectory being almost perpendicular to our line of sight. This provides an opportunity to better study the dynamics of large cluster collisions. The Chandra observations revealed that the primary baryonic component had been stripped away in the collision and resided between the two clusters in the form of hot X-ray emitting gas. This provides strong evidence for the existence of dark matter for the following reasons. As the two clusters passed through each other, the baryonic components of these two clusters interacted and slowed down due to ram pressure. However the dark matter component was allowed to move ahead of the gas, because it only interacts through gravity. One can infer the velocity of the bow shock preceding the 'bullet' through the shock Mach number and a measurement of the pre-shock temperature. The inferred shock velocity is found to be $v_{\rm shock}=4740^{+710}_{-550}$ km s^{-1}(Markevitch, 2006; Springel & Farrar, 2007).

It is often assumed that the inferred shock velocity is equal to the velocity of the dark matter 'bullet' itself. This high speed provides a challenge to the ΛCDM model since it does not predict such high relative velocities. Several groups have shown, however, that this is not necessarily the case through the use of non-cosmological hydrodynamic simulations. Milosavljević et al. (2007) used two dimensional simulations to find that the subcluster's velocity differed from the shock velocity by about 16%, bringing the relative velocity down to ∼3980 km s^{-1}. They assumed a zero

relative velocity at a separation distance of 4.6 Mpc for their initial conditions. They also emphasized that their conclusion is sensitive to the initial mass and gas density profile of the two clusters. Later Springel & Farrar (2007) showed through the use of three dimensional hydrodynamic toy models that the subcluster's relative velocity could be as low as $\sim$2700 km s^{-1}. Their initial conditions assumed a relative velocity of 2057 km s^{-1} at a separation distance of 3.37 Mpc. Mastropietro & Burkert (2008) explored a larger range of initial relative velocities at initial separation distances of 3.37 Mpc and 5Mpc through the use of three dimensional hydrodynamic simulations. They found that in order to accurately reproduce the observational data of 1E0657-56, a relative halo infall velocity of $\sim$3100 km s^{-1} at an initial distance of 5 Mpc was required.

Lee & Komatsu (2010) quantified the likelihood of finding bullet-like systems in the large cosmological simulation MICE (Crocce et al., 2010). They examined DM halos at redshifts of z=0.5 & z=0, concluding that the ΛCDM model is incompatible with observations of 1E0657-56 at a 99.95% confidence level for z=0. At z=0.5 however, their results were not fully conclusive due to limited statistics. They estimated the probability of finding such a system at z=0.5 to be 3.6×10^{-9} if the distribution is indeed Gaussian, but warn that these estimates may be inaccurate because they are probing the tail of the distribution.

We examine ΛCDM N-body simulations to see how common these high relative velocities are among massive DM halos. This paper is organized as follows. Section 2 discusses simulation parameters and how the overall resolution is calculated and adjusted. Section 3 dives into the simulation results and addresses specific parameters relevant to this study. Subsection 3 examines the importance of simulation results at z=0.296 and how they relate to the bullet system. Finally Section 4 contains my concluding remarks and discussion of future prospects.

CHAPTER 2

SIMULATIONS

For our simulations we use the GADGET-3 code (as originally described in Springel, 2005) which simulates large N-body problems by means of calculating gravitational interactions with a hierarchical multipole expansion, and gas dynamics (if present) are followed with smoothed particle hydrodynamics (SPH). The gravity is solved in two parts: the short-range forces are calculated by a tree technique, and the long-range forces are computed with a FFT-based particle mesh scheme.

Cosmological parameters consistent with the cosmological constraints from the Wilkinson Microwave Anisotropy Probe (WMAP) data were employed when creating the initial conditions for each simulation: ($\Omega_{\rm m}$, Ω_Λ, H_0, σ_8, n_s)$\approx$(0.26, 0.74, 72, 0.8, 1.0) (Komatsu et al., 2009, 2010). Here σ_8 measures the amplitude of the power spectrum; and n_s is the primordial power spectrum of mass density fluctuations. The value of n_s governs how the primordial matter density field fluctuates on small scales, and it dictates the amount of small scale structures. We note that we used a value of n_s=1.0 although the best-fit value from the WMAP data is n_s=0.96. Since we are mainly interested in high mass halo pairs, a slight change in n_s would have a minimal impact on the results of this study. We will check this by running a few simulations with n_s=0.96 at a later time.

Our initial conditions all employ a different number of particles (N) whose initial positions were set so that the initial density field fluctuation has a random Gaussian phase. Each simulation contains only collisionless dark matter particles that interact solely through gravity. It is useful to calculate the mass of each dark matter particle ($M_{\rm dm}$), which defines the mass resolution of each simulation. To do this, we first use Equation (1.4), Equation (1.3), and $\Omega_{\rm m}$=0.26 to solve for the current matter density in terms of solar masses per unit volume, arriving at a value of ρ_m=7.21 $\times$ 10^{10} $h^2 M_\odot {\rm Mpc}^{-3}$. To find the mass of each dark matter particle, we multiply ρ_m by

the volume of our simulation box (V), then divide the resulting value by the total number of particles:

$$M_{\rm dm}\ [h^{-1}M_{\odot}] = \frac{\rho_m\ V}{N}. \tag{2.1}$$

Lastly we define the gravitational softening length. As particles in our simulation approach one another, the force between them calculated by Newton's universal law of gravity (F=$GMmr^{-2}$) goes to infinity. This will produce unrealistic accelerations within the simulation. In order to avoid these unwanted accelerations we replace r^{-2} with $(r+\epsilon)^{-2}$, where ϵ is a small number called the gravitational softening length. This added value essentially 'softens' the gravity at small separations, and smooths out the small scale structures in our simulations. It is and is typically calculated using the following empirical rule of thumb:

$$\epsilon\ [h^{-1}{\rm kpc}] = \left(\frac{\rm V}{\rm N}\right)^{1/3} \times \frac{1}{25}, \tag{2.2}$$

where 1/25 is a fraction of the mean inter-particle separation. The value of ϵ represents the spatial resolution of a given simulation.

Several simulations with varying particle counts and box sizes were ran from the early universe (z=100) to the present time (z=0) where z is the cosmological redshift defined by Equation (1.2). The list of simulations along with their box sizes, total particle counts, gravitational softening lengths, friends-of-friends linking lengths, and mass resolutions can be found in Table 1. We started with the L250N125 simulation, and increased the box size and particle count in order to maintain the same mass resolution and gravitational softening length up to the L2000N1000 simulation. The second set of simulations were ran to examine the resolution effect. We started with the same L250N125 simulation and increased the particle count and decreased the gravitational softening length while keeping the box size the same, up to the L250N500 simulation. After the initial data analysis was complete the L2000N1000 simulation

was ran once again, this time dumping an output file at z=0.296 to see how going back in time would affect the results, which will be discussed in section 3.

CHAPTER 3

DATA ANALYSIS & RESULTS

Halo Mass Function

The simulation output files only contain particle locations and velocities. In order to properly interpret this data the particles need to be grouped into halos. This is done using the parallel friends-of-friends group finder SUBFIND (Springel et al., 2001). The code first separates the particles into groups if they lie within a specified linking length (FoF LL). This linking length is a fraction of the mean initial inter-particle separation in which we will consider a region to be over-dense. The standard linking length of 0.2 is employed in our studies. In order to be considered a halo it must also contain at least 32 particles. The code then analyzes each group for gravitationally self-bound substructures and separates them from what is then considered the background group. For each gravitationally self-bound group a center-of-mass position and the number of particles contained within the group is returned. Now that the number of particles in each group is known we can simply multiply that number by $M_{\rm dm}$ (DM particle mass listed in Table 1) to arrive at the total mass of each halo ($M_{\rm halo}$).

Figures 1 and 2 show DM halo mass functions, which presents the number density of halos occupying each mass bin. The mass of the smallest halo we expect to find in each simulation is $32\times M_{\rm dm}$. Figure 1 shows that by increasing the box size from 250 h^{-1}Mpc to 2000 h^{-1}Mpc while maintaining the same resolution, the number of high mass halos increase. The mass of the smallest halo in all simulations shown in Figure 1 is $M_{\rm halomin}$=$1.84\times10^{13}M_{\odot}$. The run with the largest box size (L2000) shows a slight shortage in the number of low mass halos around $M_{\rm halo}\simeq 10^{13.24-14.20}M_{\odot}$ when compared to the other three runs with smaller box sizes. The most likely explanation for this shortage is that the lower mass halos were absorbed into higher mass halos.

Figure 2 shows how increasing the resolution of the simulation while keeping the

box size constant increases the number of lower mass halos. Increasing the particle number decreases the gravitational softening length and increases the mass resolution at the same time, hence improving our overall resolution. Higher resolution runs can resolve smaller halos as seen in Figure 2. The smallest halo for the highest resolution simulation (L250N500) has a mass of $M_{\rm halomin}$=$2.87 \times 10^{11} M_{\odot}$, which is roughly two orders of magnitude lower than the lowest mass halos found in Figure 1.

Searching for a bullet cluster-like pair of halos with masses on the order of $M_{\rm bullet}$ & $M_{\rm parent}$, Figures 1 & 2 indicate that it is possible to form such massive halos in box sizes as small as 250 h^{-1}Mpc. Simply producing high mass halo pairs is not enough to reproduce the bullet cluster as we will see through later analysis of halo distance & pairwise velocities.

Pairwise Distance

Before examining the pairwise velocity of halos in large simulations, it is important to take the distance between them into consideration. The larger the distance between two halos, it is less likely that they are an actual pair. To see how large the halos in our simulations are, we determine the maximum radius of each halo from the center-of-mass. Many large halos were found to have radii up to $10\,h^{-1}$Mpc as seen in Figure 3, which shows the maximum halo radius as a function of its mass contained within our largest run at z=0. The red dashed line represents the virial radius of a DM halo with a given mass, at which the mean enclosed density is 200 times the critical density (Mo & White, 2002):

$$r_{\rm virial} = \left[\frac{GM}{100\ \Omega_{\rm m}(z)\ H^2(z)} \right]^{1/3}. \tag{3.1}$$

Here $H(z)$ is the Hubble parameter, and $\Omega_{\rm m}(z)$ is the density parameter at redshift z. These values are related to their present-day values (subscript 0) by:

$$H(z) = H_0 E(z) \quad \text{and} \quad \Omega_{\rm m}(z) = \frac{\Omega_{\rm m,0}(1+z)^3}{E^2(z)}, \tag{3.2}$$

where

$$E(z) = \left[\Omega_{\Lambda,0} + \Omega_{\rm m,0}(1+z)^3\right]^{1/2}. \tag{3.3}$$

It is clear that the maximum radius increases with increasing virial radius. The approximate virial radii of 1E0657-56 at z=0.296 is $r_{\rm virial}\simeq$2.80 Mpc for the parent, and $r_{\rm virial}\simeq$1.30 Mpc for the bullet. To be conservative all pairs with a distance between their centers of mass smaller than $10\,h^{-1}$Mpc were considered.

Care must be taken as to not double count the number of pairs. Two identical lists of halos denoted i and j were created to allow for easy comparison. We first define the distance between the center-of-mass of each respective halo pair by:

$$d = \sqrt{dX_{ctr}^2 + dY_{ctr}^2 + dZ_{ctr}^2}, \tag{3.4}$$

where dX_{ctr}=$(xctr_i - xctr_j)$, dY_{ctr}=$(yctr_i - yctr_j)$, and dZ_{ctr}=$(zctr_i - zctr_j)$. We then compare $halo_{i=1}$ to $halo_{j=i+1}$ through $halo_{j=i+(n-1)}$, where n represents the total number of halos. We repeat this calculation until evaluating the comparison for $halo_{i=n-1}$. This process allows us to get a single value for the distance between each halo pair within the limiting distance without double counting.

Pairwise Velocity Distribution Function

Knowing each group's absolute velocity components with respect to the simulation box makes it rather simple to calculate their pairwise velocities (v_{12}). By defining dv_x=$(v_{xi} - v_{xj})$, dv_y=$(v_{yi} - v_{yj})$, and dv_z=$(v_{zi} - v_{zj})$, we calculate each group's pairwise

velocity:

$$v_{12} = \sqrt{dv_x^2 + dv_y^2 + dv_z^2}, \tag{3.5}$$

using the same comparison methodology described in the previous section to avoid double counting.

Figures 4 & 5 show the number of halo pairs within a velocity bin per unit volume. Both Figures are separated into four panels, each showing the results from the simulation name printed in the top right corner. Each panel is then broken down into three lines showing halo pairs with a separation distance of less than $2, 5, \ \& \ 10 \ h^{-1}$Mpc.

Figure 4 displays how increasing the box size while maintaining resolution allows for more high velocity halo pairs. The majority of the higher velocity pairs have a separation distance of $5-10 \ h^{-1}$Mpc, which makes it difficult to tell if they are actual pairs or not. It appears to be a trend that the closer the halo pair is, the lower its pairwise velocity. The high pairwise velocity for largely separated pairs is probably due to the large-scale bulk motion of physically separated structures.

Figure 5 shows the resolution effect on the velocity distribution function while keeping the box size the same. We find that as we increase the resolution, we see more high velocity pairs. Unlike the previous case, as we increase the resolution the higher velocity halo pairs seem to stick closer together. This may very well be due to the limited box size, but further investigation would be needed in order to draw this conclusion.

Given the bullet cluster's separation distance of $d \simeq 0.72\,$Mpc, it is already apparent that in order to produce such a close and high pairwise velocity pair one would need a large box size with a higher resolution.

Relative Halo Velocity & Halo Mass

We compare the masses of our high velocity halo pairs to the observed masses of the bullet cluster and its parent. For this it is useful to plot the average mass of a

halo pair vs. their pairwise relative velocity as shown in Figures 6 & 7. For reference the average mass of the bullet cluster and its parent cluster is $\log\langle \mathrm{M}\rangle \simeq 14.92\, M_{\odot}$, illustrated in the figures by the dashed gray line.

Figure 6 shows how increasing the box size with a constant resolution not only increases the number of low-mass, high velocity halo pairs, but it also increases the number of high mass high velocity pairs. Even with the largest box size simulation (L2000) the pairs of interest only reach relative speeds upwards of $v_{12}{\simeq}2000\,\mathrm{km\,s^{-1}}$, with maximum pairwise velocities reaching $v_{12}{\simeq}3000\,\mathrm{km\,s^{-1}}$ for low-mass pairs. This difference of roughly $1000\,\mathrm{km\,s^{-1}}$ present between the higher velocity low mass pairs and higher velocity high mass pairs also seems to be a trend in each of the smaller box simulations.

Figure 7 shows the resolution effects. A higher resolution results in more low mass high velocity pairs and fewer high mass high velocity pairs. It is also clear from the bottom panel of this Figure that we have hit our high mass limit of approximately $10^{15} M_{\odot}$ in agreement with Figure 2. This means that, if we want to probe higher mass halos while improving the resolution, we must also increase the box size. Even our highest resolution simulation with average halo masses approaching that of the bullet system are still only found to have relative velocities on the order of $v_{12}{\simeq}1800\,\mathrm{km\,s^{-1}}$. It can also be seen from this figure that as we increase our resolution, we are probing the pairwise velocities of lower mass halos. In the top panel (L250N125) of Figure 7 the lowest value is $\langle \mathrm{M}\rangle \simeq 10^{13.30} M_{\odot}$, where as in the bottom panel (L250N500) the lowest value is $\langle \mathrm{M}\rangle \simeq 10^{11.40} M_{\odot}$. It would seem as though arbitrarily increasing the resolution may be a waste of computational resources as the number of high mass high velocity halo pairs found through increasing resolution is quite low when compared to increasing the box size.

Cumulative Halo Velocities

To examine how the box size and resolution affects the number of high velocity halo pairs, we simply count the cumulative number of pairs above a certain velocity as shown in Figures 8 & 9. Figure 8 shows how increasing the overall resolution of simulation affects the slope of this cumulative distribution. More high velocity halo pairs are produced as we increase the resolution as seen in Figure 5, but we know that these high velocity pairs are relatively low mass and not the pairs we are searching for from Figure 7. Figure 9 shows that as we increase the box size, we extend the curve to larger pairwise halo velocities. Assuming that this trend will continue, we fit a quadratic to the curve of our largest simulation (L2000N1000) of the form $f{=}y_0 + ax + bx^2$ (where $x{=}v_{12}$ & $y{=}\log dN(>v_{12})/dV$). This allows us to estimate what box size simulation at this redshift ($z{=}0$) and resolution would be needed to produce a single pair of halos with a relative velocity of 4740 km s^{-1}(Markevitch, 2006), 3980 km s^{-1}(Milosavljević et al., 2007), 3100 km s^{-1}(Mastropietro & Burkert, 2008), and 2700 km s^{-1}(Springel & Farrar, 2007). The curve was fitted between the velocities 1000 and 2500 as indicated by the black dashed lines in Figure 10 with resulting values of $y_0{=}-3.1386$, $a{=}-2.3359 \times 10^{-3}$, $b{=}1.1278 \times 10^{-7}$. Using the fitted function, we find the points marked by '+' on Figure 10 at (x, y)=(4740,-11.68),(3980,-10.65),(3100,-9.30), and (2700,-8.62) translating to box sizes of $L_{box}{\sim}$3612, 2657, 1689, & 1315 h^{-1}Mpc respectively. In order to maintain the same resolution, simulations with these box sizes would require $N{\simeq}1806^3, 1329^3, 845^3, \& \ 658^3$ particles. Given these results, our largest simulation should contain candidate bullet-like pairs consistent with the requirements of Mastropietro & Burkert (2008); Springel & Farrar (2007). But as before, their masses are too low to be consistent with 1E0657-56 observations.

Halo Pair Velocity Angles

Given the large separation distance between many of the high velocity halo pairs it is difficult to tell if they are actual pairs. Another parameter that gives us a better idea of their orientations is the angle between their velocity vectors. Knowing this angle can assist us in determining if high velocity pairs have velocity vectors directed towards each other or not. We calculate the angle between a pair by taking the dot product of the pair's velocity vectors and solving for the angle as

$$\theta = \cos^{-1} \frac{\vec{v_i} \cdot \vec{v_j}}{|v_i||v_j|}. \tag{3.6}$$

Unfortunately the angle itself does not tell us if the two halos are heading towards or away from one another. Further investigation into the pair's position and velocity vectors would need to be performed to determine this for the close pair candidates.

Results at Redshift z=0.296

To be fully consistent with 1E0657-56, comparing simulation data from the same time period would be ideal. Up until this point all of the simulation data has been from the era of z=0, yet the bullet system is observed at a redshift of z=0.296. This difference in time of ∼3.32 billion years (Wright, 2006) can have a considerable impact on the velocities, sizes, and separation distances of the halos contained within the simulation.

The largest simulation (L2000N1000) was re-ran up until a redshift of z=0.296 where an output file was then dumped. The halos were then grouped, then their radii and distances were calculated as described by previous sections. The same limiting distance of 10 h^{-1}Mpc was chosen. Finally pairwise velocities were calculated, then multiplied by $\sqrt{a}$ to correct for the redshift effect. The top panel of Figure 11 shows the same velocity function from the bottom panel of Figure 4 at z=0 compared to

the velocity function of the same simulation at z=0.296. We see here that as we go back to earlier redshifts pairwise velocities greatly increase. Pairs within separation distances of 2 h^{-1}Mpc now have maximum pairwise velocities on the order of $\simeq$3000 km s^{-1}, and as their separation distances increase we reach pairwise velocities as high as $\simeq$7500 km s^{-1}. Figure 12 compares the same velocity vs. average halo mass plot from the bottom panel of Figure 6 at z=0 to the results from the same simulation at z=0.296 in the bottom panel. The number density of halo pairs in the area of interest has greatly increased. Unfortunately further investigation reveals that their mass ratios are not in agreement with the observational properties of 1E0657-56.

CHAPTER 4

DISCUSSION & CONCLUSIONS

Many N-Body simulations with varying box sizes and resolutions were run in order to examine how changing these parameters affect the search for high velocity halo pairs comparable to the 'bullet' in the 1E0657-56 system. Properties of halos from the L2000N1000 simulation were chosen because of its large box size and moderate resolution. Much of the data presented in this work is from simulations ran up until present day (z=0), but the largest simulation was re-run until z=0.296. The important properties reviewed were pairwise velocities, halo masses, and halo separation distance. Halo distances, and radii for the z=0.296 data were all corrected for the redshift effect by dividing their co-moving values returned by the simulation by $(1 + z)$.

Table 2 lists the ten largest averaged halo mass pairs for the z=0 and z=0.296 case. A simulation of this size only creates a few halo pairs massive enough to match 1E0657-56 observations at z=0 and z=0.296. In the z=0 case the pairwise velocities are too low to match up to the required 3100 km s^{-1} (Mastropietro & Burkert, 2008), but at z=0.296 we see that their pairwise velocities have greatly increased with seven pairs easily reaching and even exceeding 3100 km s^{-1}. Unfortunately the separation distances of all halo pairs in this table are much larger than the observed separation distance of d$\simeq$0.72 Mpc for the bullet system. Pair 20 is a close match to the initial condition requirements of Mastropietro & Burkert (2008) with a pairwise velocity of $\simeq$3135 km s^{-1}, but with an average mass of $\simeq 10^{15.61} M_{\odot}$ the halos are too large.

Table 3 lists the ten closest halo pairs for the z=0 and z=0.296 case. All of these pairs are quite close in agreement with the observations of 1E0657-56, but their masses and relative halo velocities fall severely short of the halos we are searching for.

Table 4 lists the ten highest pairwise velocity halos for z=0 and z=0.296. Here we see that all of the halos listed have relatively large separation distances and low

masses when compared to $M_{\rm bullet}$ & $M_{\rm parent}$. As we saw in Figure 1 we would need to greatly increase the box size to allow for higher mass halos, but at the same time we would have to greatly increase the resolution to lower the separation distance as seen in Figure 5 for the z=0 case. For the z=0.296 case we see that the 10 highest pairwise velocity halos greatly exceed the required velocity of 3100 km s^{-1}. Here their masses are too small to match observations, and their separation distances are once again too large.

The list of halos in the L2000N1000 z=0.296 simulation was mined looking for bullet-like pairs only considering their masses, mass ratios, pairwise velocities, and separation distances. A table of the top five pairs that most closely resembled the observational properties of 1E0657-56 including the v_{12} requirement of 3100 km s^{-1} (Mastropietro & Burkert, 2008) is found in Table 5. After calculating the angle between their velocity vectors it is clear that pair 61 is not on a near head-on trajectory, while pairs 62, 63, 64, and 65 all have trajectory angles approximately $\sim$60° off from being head on. The masses of pairs 61-65 are all about a factor of ten too small, and have relatively large separation distances when compared to observations. Future plans include increasing the simulation box size to allow for better high mass halo statistics.

It is quite a challenge to reproduce the observational properties of 1E0657-56 in N-body simulations. One has to produce halos pairs of the appropriate masses and mass ratios, relatively high pairwise velocities with near head on collision angles, and the appropriate separation distance between the halo pairs. In my studies I found it very unlikely that one could produce such a halo pair at z=0, but at z=0.296 the situation became less unlikely due to the dramatic increase in pairwise velocities. Unfortunately the masses and separation distances of the pairs still proved to be incompatible with the observational properties of 1E0657-56. It does seem possible however, that one can produce the initial conditions required by Mastropietro &

Burkert (2008) to create such a 'bullet'. Pair 65 in Table 5 is a prime example of such a pair; with a relative velocity of $\sim$3100 km s^{-1} and a separation distance of $\sim$4.6 h^{-1} Mpc it only differs from the initial conditions of Mastropietro & Burkert (2008) by the pair's mass being a factor of $\sim$10 too low, and that the collision angle is $\sim$60° from being head on.

It is also entirely possible that a bullet-like cluster is nested within one of our large halos but were were unable to locate it due to the specified linking lengths for the friends-of-friends grouping algorithm used throughout this study. In the future we plan on decreasing the linking length in hopes of finding such a nested cluster. We also plan to re-run each simulation to z=0.296 to see if the trends present at z=0 are also present at higher redshifts. It may also be useful to examine simulations at a redshift earlier than z=0.296 to see if the ΛCDM model can reproduce halo pairs with conditions similar to the initial conditions of Mastropietro & Burkert (2008) that reproduced the observational properties of 1E0657-56. In the future we plan on statistically quantifying the likelihood of finding such a halo pair at various redshifts. If we find the ΛCDM model to be consistent with observations, it is clear from this study alone that events such as 1E0657-56 are quite rare.

Table 1. Summary of Simulations

Run Name	Box Size $[h^{-1}$ Mpc]	Particle Count $[\mathrm{N}]^{\frac{1}{3}}$	M_{dm} $[h^{-1}\ M_{\odot}]$	ϵ $[h^{-1}$ kpc]	FoF LL $[h^{-1}$ kpc]
Box Size Effects					
L250 N125	250	125	5.74×10^{11}	80	400
L500 N250	500	250	5.74×10^{11}	80	400
L1000 N500	1000	500	5.74×10^{11}	80	400
L2000 N1000	2000	1000	5.74×10^{11}	80	400
Resolution Effects					
L250 N125	250	125	5.74×10^{11}	80	400
L250 N165	250	165	2.50×10^{11}	60.6	303
L250 N250	250	250	7.18×10^{10}	40	200
L250 N500	250	500	8.97×10^{9}	20	100

Note. — A summary of simulations employed in this paper. ϵ is the gravitational softening length calculated using Equation (2.2), M_{dm} is the mass of each DM particle calculated using Equation (2.1), and FoF LL is the friends-of-friends linking length. The top four simulations explore the effects of increasing the box size while maintaining the same resolution, while the bottom four explore the effects of increasing the mass and spatial resolution.

Table 2. Highest Mass Pairs

Pair	v_{12}	θ	M_1	M_2	Ratio	d	$r_{1virial}$	r_{1max}	$r_{2virial}$	r_{2max}
z=0										
1	1669.65	165	5.71E+15	4.99E+14	0.087	8.70	5.67	5.84	2.52	3.40
2	1792.24	46	5.71E+15	1.99E+14	0.035	7.84	5.67	5.84	1.85	2.71
3	1766.49	75	5.71E+15	1.01E+14	0.018	7.63	5.67	5.84	1.48	2.14
4	1625.45	80	5.71E+15	7.27E+13	0.013	7.13	5.67	5.84	1.32	1.53
5	2316.36	72	5.71E+15	7.10E+13	0.012	6.21	5.67	5.84	1.31	1.52
6	1645.19	51	5.71E+15	3.87E+13	0.007	8.74	5.67	5.84	1.07	1.45
7	2062.06	95	5.71E+15	3.23E+13	0.006	8.58	5.67	5.84	1.01	0.95
8	2035.07	77	5.71E+15	2.25E+13	0.004	9.27	5.67	5.84	0.90	1.11
9	1662.06	116	4.79E+15	1.91E+13	0.004	8.19	5.35	7.33	0.85	1.50
10	1304.08	84	4.79E+15	1.91E+13	0.004	9.29	5.35	7.33	0.85	1.23
z=0.296										
11	3136.52	104	1.07E+16	3.44E+14	0.032	7.31	5.39	6.09	1.71	1.96
12	2398.52	111	1.07E+16	7.56E+13	0.007	6.90	5.39	6.09	1.03	1.61
13	3954.07	75	1.07E+16	4.56E+13	0.004	5.61	5.39	6.09	0.87	0.76
14	4109.03	44	1.07E+16	3.23E+13	0.003	5.08	5.39	6.09	0.78	0.55
15	2079.49	106	1.07E+16	2.54E+13	0.002	5.41	5.39	6.09	0.72	1.05
16	4463.41	106	1.07E+16	2.02E+13	0.002	3.05	5.39	6.09	0.67	0.75
17	3857.40	32	8.15E+15	8.43E+13	0.010	4.74	4.92	6.04	1.07	0.98
18	3629.31	91	8.15E+15	7.04E+13	0.009	4.84	4.92	6.04	1.01	0.96
19	2687.07	128	8.15E+15	6.87E+13	0.008	6.42	4.92	6.04	1.00	1.05
20	3135.90	141	7.53E+15	6.99E+14	0.093	6.73	4.80	10.86	2.17	3.04

Note. — The ten largest average halo mass pairs from the L2000N1000 simulation at z=0 and z=0.296. While a simulation of this box size can produce pairs matching observations of 1E0657-56 it is important to note their low relative velocities for the z=0 case, and large separation distances for both cases. v_{12} is given in km s^{-1}, masses are given in $M_\odot$, distances (d) and radii given in h^{-1}Mpc.

Table 3. Closest Pairs

Pair	v_{12}	θ	M_1	M_2	Ratio	d	$r_{1virial}$	r_{1max}	$r_{2virial}$	r_{2max}
z=0										
21	320.99	60	2.08E+13	1.96E+13	0.944	0.70	0.87	1.05	0.86	1.04
22	526.04	84	2.25E+13	1.96E+13	0.872	0.82	0.90	0.74	0.86	0.65
23	309.09	84	5.14E+13	1.96E+13	0.382	0.87	1.18	1.48	0.86	1.38
24	422.42	40	2.25E+13	2.08E+13	0.923	0.92	0.90	0.78	0.87	0.88
25	94.89	10	5.72E+13	2.89E+13	0.505	0.92	1.22	2.21	0.97	0.89
26	330.83	60	3.06E+13	2.54E+13	0.830	0.92	0.99	1.15	0.93	0.84
27	211.55	29	7.33E+13	2.14E+13	0.291	0.95	1.33	1.82	0.88	1.44
28	342.82	45	2.08E+13	1.91E+13	0.917	0.96	0.87	1.33	0.85	0.95
29	127.37	6	2.66E+13	1.91E+13	0.717	0.97	0.95	0.70	0.85	1.27
30	252.72	19	1.91E+13	1.91E+13	1.000	0.98	0.85	0.81	0.85	0.74
z=0.296										
31	411.14	12	2.25E+13	1.91E+13	0.849	0.57	0.69	0.36	0.65	0.94
32	232.86	11	4.04E+13	2.14E+13	0.530	0.58	0.84	0.60	0.68	0.95
33	334.68	25	2.37E+13	2.08E+13	0.878	0.61	0.70	0.72	0.67	0.59
34	671.93	47	2.02E+13	1.91E+13	0.946	0.61	0.67	0.48	0.65	0.46
35	678.21	12	2.66E+13	2.25E+13	0.846	0.61	0.73	1.03	0.69	0.63
36	614.99	47	3.46E+13	2.42E+13	0.699	0.62	0.80	0.38	0.71	0.79
37	336.38	24	2.89E+13	2.02E+13	0.699	0.64	0.75	0.89	0.67	0.48
38	581.28	73	2.25E+13	1.91E+13	0.849	0.65	0.69	0.57	0.65	0.70
39	724.55	50	2.08E+13	2.02E+13	0.971	0.66	0.67	0.65	0.67	0.64
40	835.49	31	2.37E+13	1.91E+13	0.806	0.66	0.70	0.61	0.65	0.47

Note. — The ten closest halo pairs in the L2000N1000 simulation for z=0 and z=0.296. All of these pairs are close to the observed separation distance of 1E0657-56 but all have very low relative velocities and masses. v_{12} is given in km s^{-1}, masses are given in $M_\odot$, distances (d) and radii given in h^{-1}Mpc.

Table 4. Highest Velocity Pairs

Pair	v_{12}	θ	M_1	M_2	Ratio	d	$r_{1virial}$	r_{1max}	$r_{2virial}$	r_{2max}
z=0										
41	3673.46	103	3.64E+13	2.71E+13	0.746	8.83	1.05	1.06	0.95	1.28
42	3199.25	151	2.14E+13	2.02E+13	0.946	8.20	0.88	0.80	0.86	0.86
43	3132.84	134	5.83E+13	2.60E+13	0.446	9.09	1.23	1.36	0.94	1.17
44	3094.64	114	8.20E+13	4.56E+13	0.556	9.21	1.38	1.72	1.13	1.35
45	3053.49	108	8.20E+13	2.14E+13	0.261	9.11	1.38	1.72	0.88	1.36
46	2943.54	148	5.43E+13	2.54E+13	0.468	8.38	1.20	1.47	0.93	1.00
47	2921.13	158	1.67E+14	2.14E+13	0.128	7.83	1.75	2.10	0.88	0.97
48	2919.17	126	3.93E+13	3.93E+13	1.000	9.43	1.08	0.88	1.08	1.15
49	2916.59	135	3.81E+13	2.94E+13	0.773	9.27	1.07	0.99	0.98	1.05
50	2888.64	173	2.83E+13	2.71E+13	0.959	6.92	0.97	1.04	0.95	1.36
z=0.296										
51	7447.37	127	4.56E+13	2.02E+13	0.443	6.73	0.87	0.76	0.67	0.75
52	7385.98	139	7.04E+13	4.33E+13	0.615	7.35	1.01	0.96	0.86	0.93
53	6769.60	109	4.33E+13	4.16E+13	0.961	7.34	0.86	0.93	0.85	0.75
54	6480.53	123	4.33E+13	1.96E+13	0.453	7.34	0.86	0.93	0.66	0.87
55	6159.14	118	7.04E+13	3.00E+13	0.426	6.60	1.01	0.96	0.76	0.58
56	6052.69	141	3.23E+13	2.54E+13	0.786	2.74	0.78	0.55	0.72	1.05
57	6007.81	134	4.27E+13	1.85E+13	0.433	6.03	0.86	1.06	0.65	0.60
58	5922.04	102	8.43E+13	2.25E+13	0.267	5.02	1.07	1.27	0.69	0.79
59	5883.44	87	4.56E+13	3.23E+13	0.708	5.64	0.87	0.76	0.78	0.55
60	5780.16	135	7.91E+13	4.16E+13	0.526	6.38	1.05	0.88	0.85	0.76

Note. — The ten highest pairwise velocity halos found in the L2000N1000 simulation at z=0 and z=0.296. None of these high velocity halo pairs are massive enough to match the observations of 1E0657-56, and they all have relatively large separation distances with small radii arguing against many of these being actual pairs. v_{12} is given in km s^{-1}, masses are given in $M_\odot$, distances (d) and radii given in h^{-1}Mpc.

Table 5. Bullet-like Pairs at z=0.296

Pair	v_{12}	θ	M_1	M_2	Ratio	d	$r_{1virial}$	r_{1max}	$r_{2virial}$	r_{2max}
61	3198.35	70	2.67E+14	2.08E+13	0.078	3.65	1.58	1.81	0.67	0.61
62	3142.82	115	2.31E+14	2.37E+13	0.103	3.03	1.50	1.45	0.70	0.60
63	3142.82	115	2.31E+14	2.37E+13	0.103	3.03	1.50	1.45	0.70	0.60
64	3140.99	127	1.12E+14	2.19E+13	0.196	3.79	1.18	1.25	0.68	0.60
65	3100.35	122	2.68E+14	3.06E+13	0.114	4.59	1.58	1.53	0.77	1.20

Note. — Bullet-like pairs at z=0.296 selected based on their pairwise velocities, masses, mass ratios, and separation distances. Pair 61 has a trajectory angle inconsistent with observations. Pair 64's mass ratio is too high compared to the observed mass ratio of ∼0.1. Pair 65 is the most likely contender although the masses of this pair are a factor of ten too low, and their separation distance is too far. v_{12} is given in km s^{-1}, masses are given in $M_\odot$, distances (d) and radii given in h^{-1}Mpc.

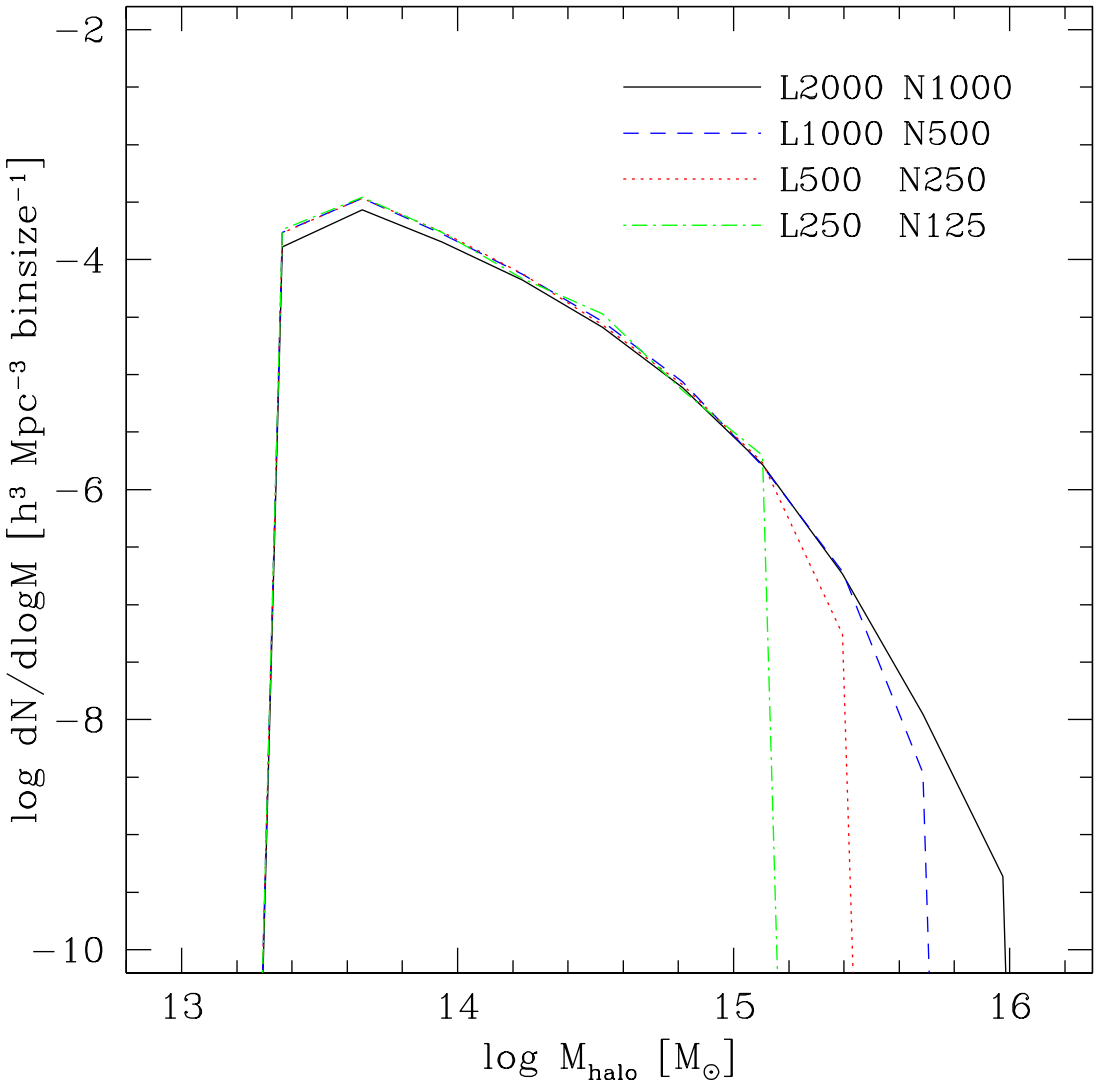

Figure 1 DM halo mass function, box size effect. This shows how increasing the box size of a simulation allows for a larger number of high mass halos. Bin size of 0.29

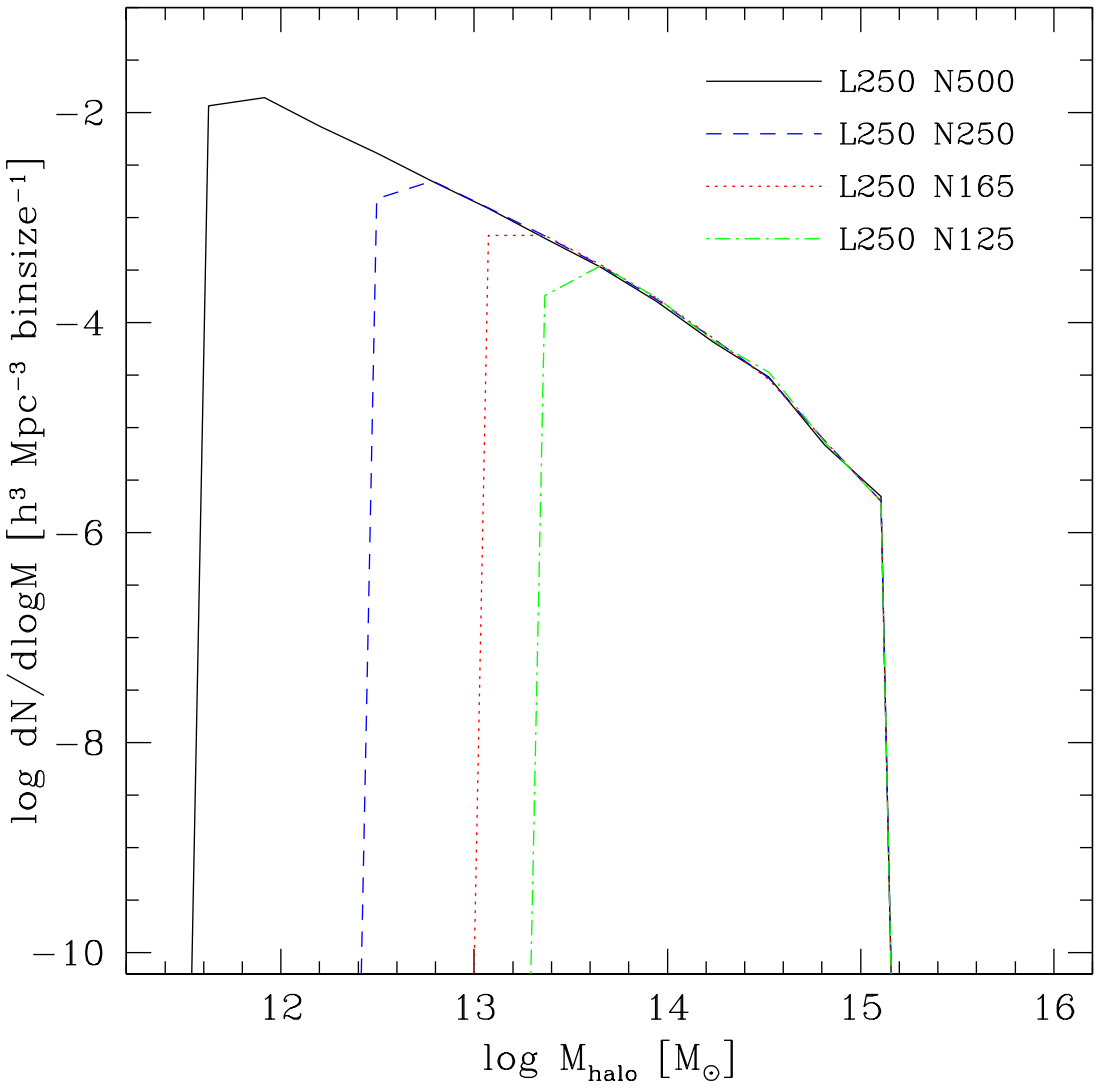

Figure 2 DM halo mass function, resolution effect. This shows how increasing the resolution of a simulation allows for a greater number of small mass halos. Bin size of 0.29

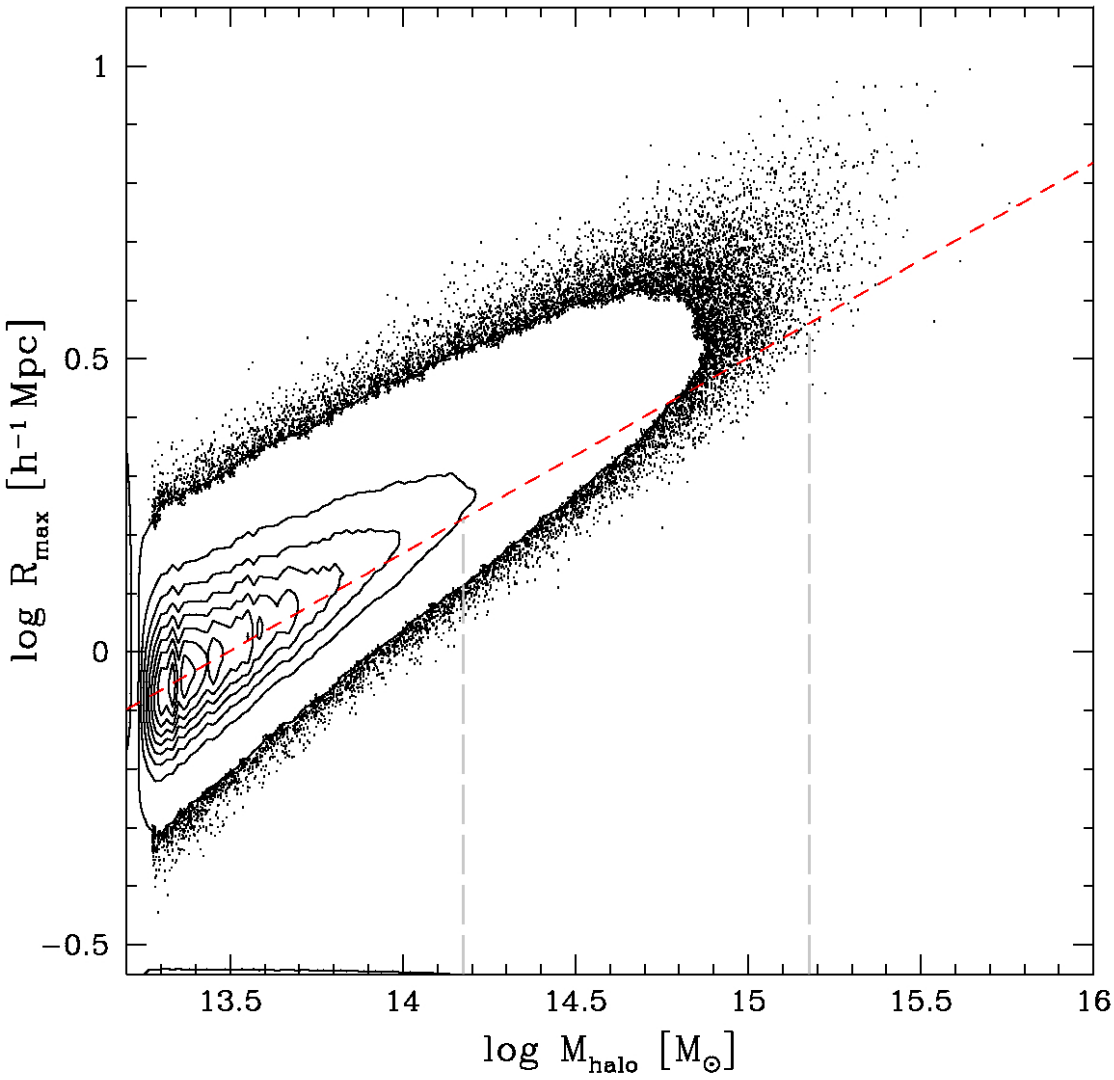

Figure 3 Maximum DM halo radius vs. DM halo mass for the L2000N1000 simulation at z=0. The red dashed line represents the virial radius calculated by Equation (3.1). We see here that as we examine higher mass halos their average radius steadily becomes larger than their virial radius. The vertical dashed lines represent $r_{\rm virial,bullet}\simeq$1.69, & $r_{\rm virial,parent}\simeq$3.63 at z=0. Halos with a radius of up to 10 h^{-1}Mpc were considered for this study.

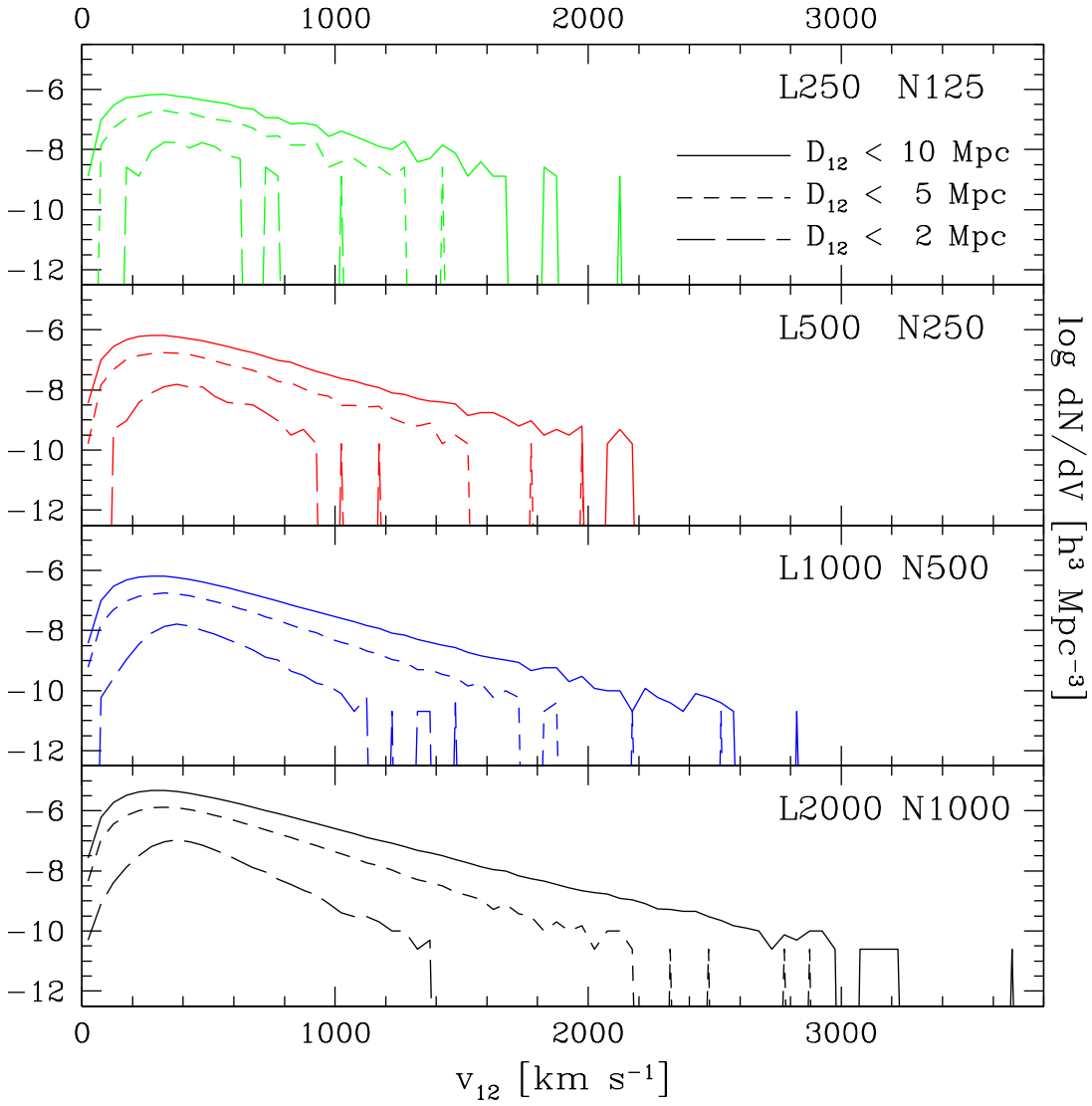

Figure 4 Velocity function, box size effect. Increasing the box size allows for higher pairwise velocities, but their separation distances increase as well.

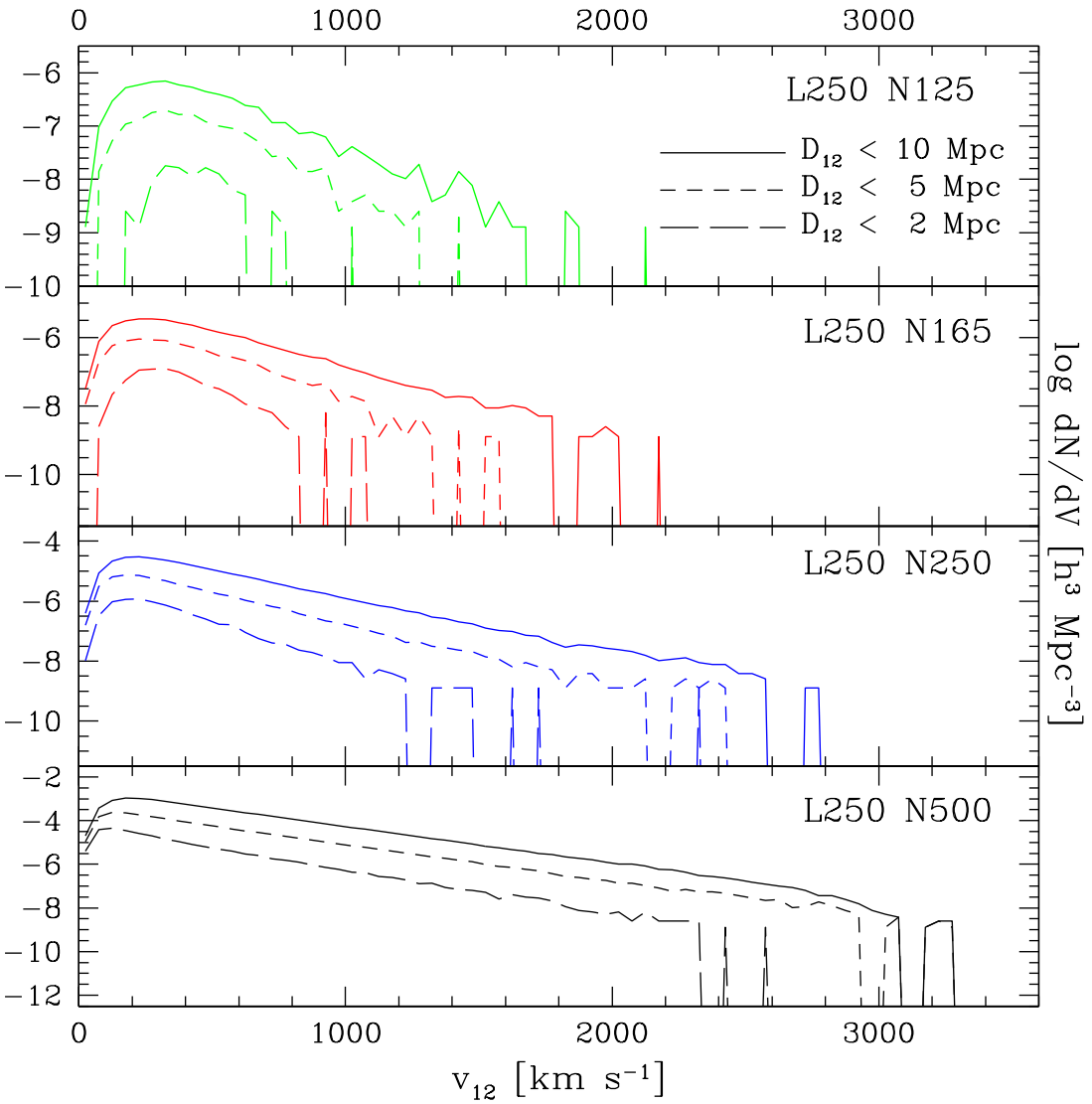

Figure 5 Velocity function, resolution effect. Increasing the resolution of the simulation allows for higher pairwise velocities, and seems to keep their separation distances close together. Although it is possible that this is due to the limited box size.

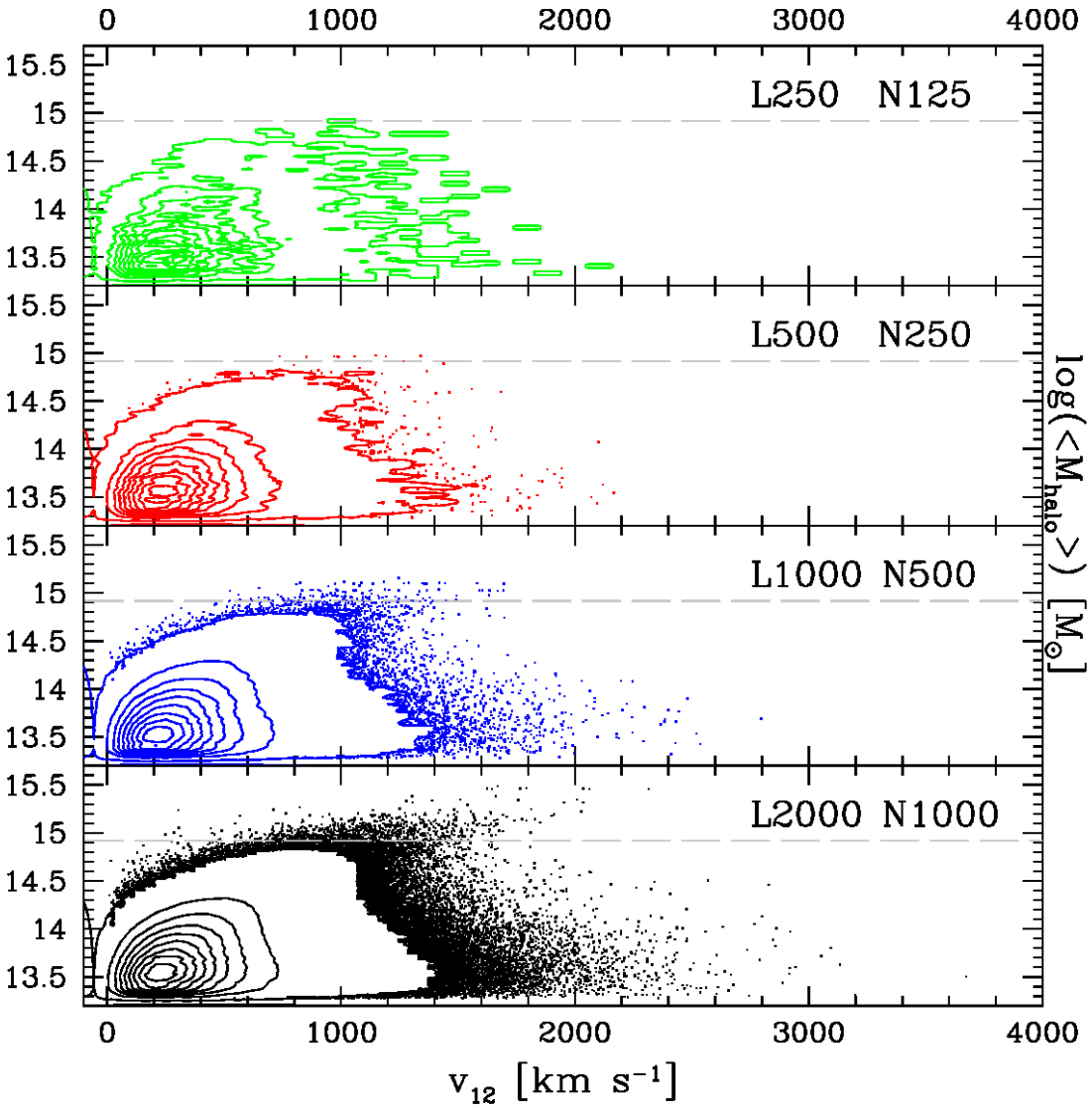

Figure 6 Velocity vs. average DM halo mass, box size effect. Increasing the simulation box size shows us that the number of low mass high velocity pairs increases more than the high mass high velocity pairs do. The horizontal dashed line represents the average mass of 1E0657-56.

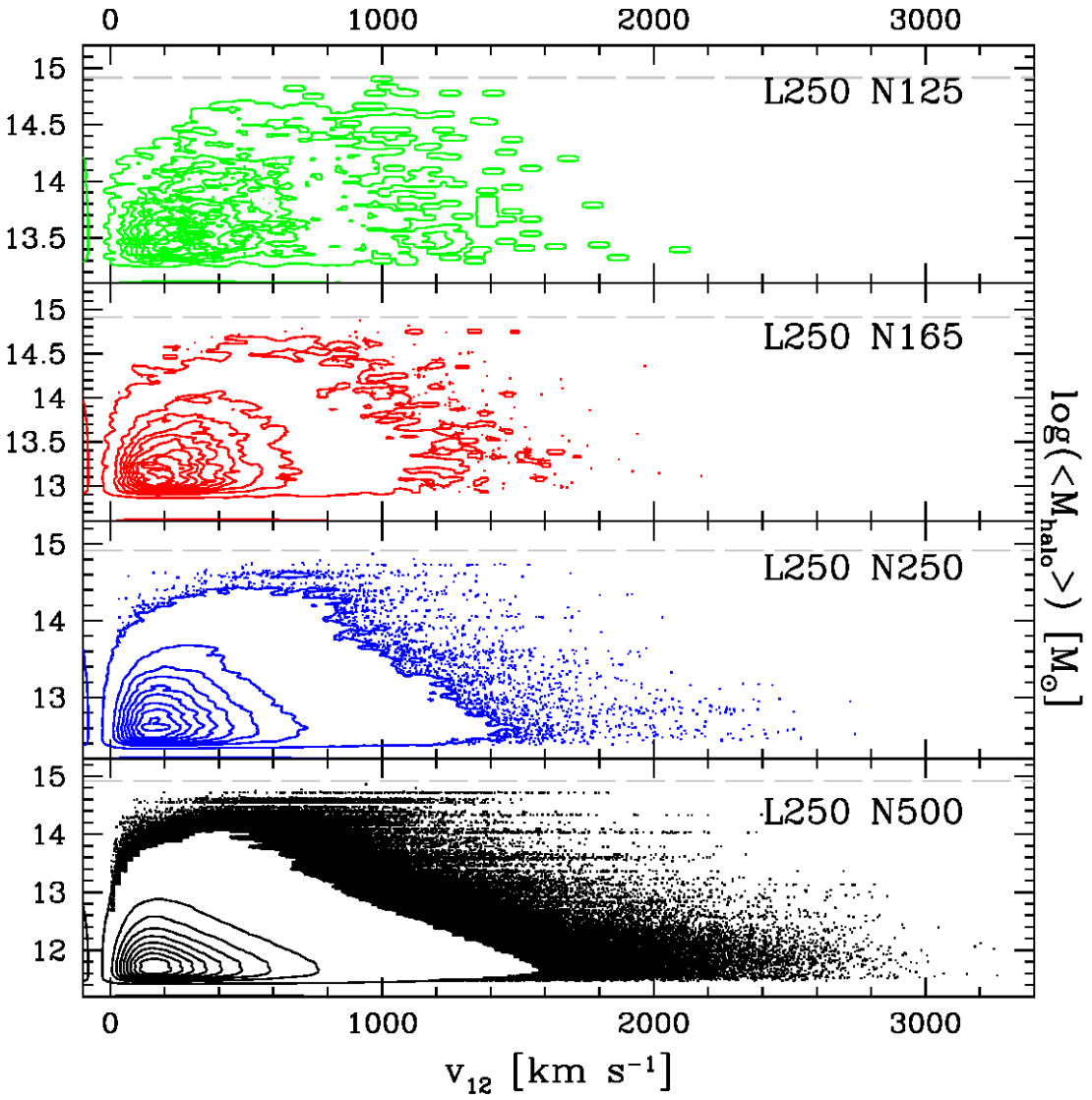

Figure 7 Velocity vs. average DM halo mass, resolution effect. Increasing the resolution probes lower mass halo pairs. There is a slight increase in high mass high velocity pairs but the majority of the increase is in the low mass regime. The horizontal dashed line represents the average mass of 1E0657-56.

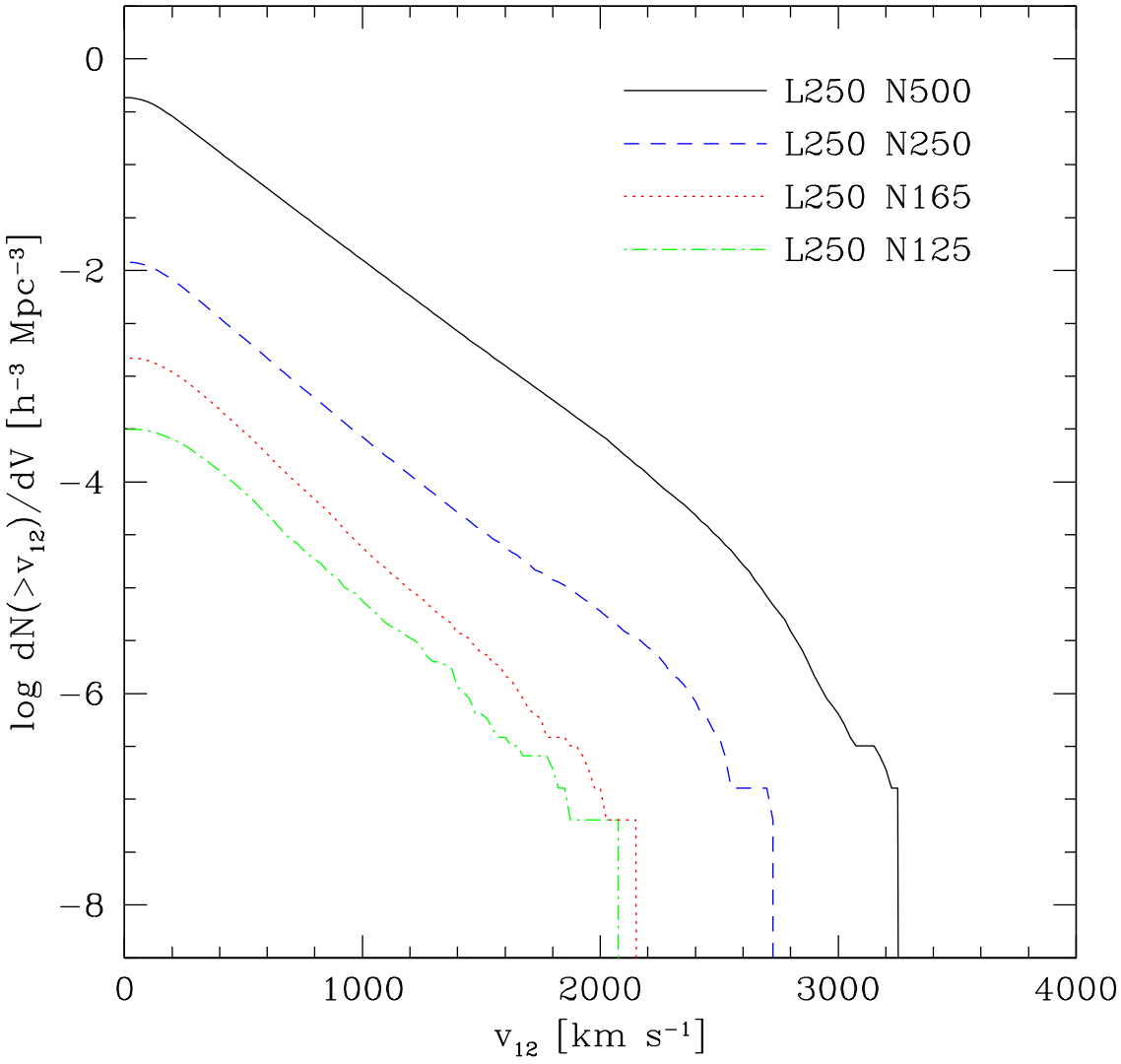

Figure 8 DM halo cumulative velocity function, resolution effect. Here we see that increasing the resolution of the simulation changes the slope of the cumulative curve. From Figure 7 we know that this increase in high velocity pairs is due to low mass pairs.

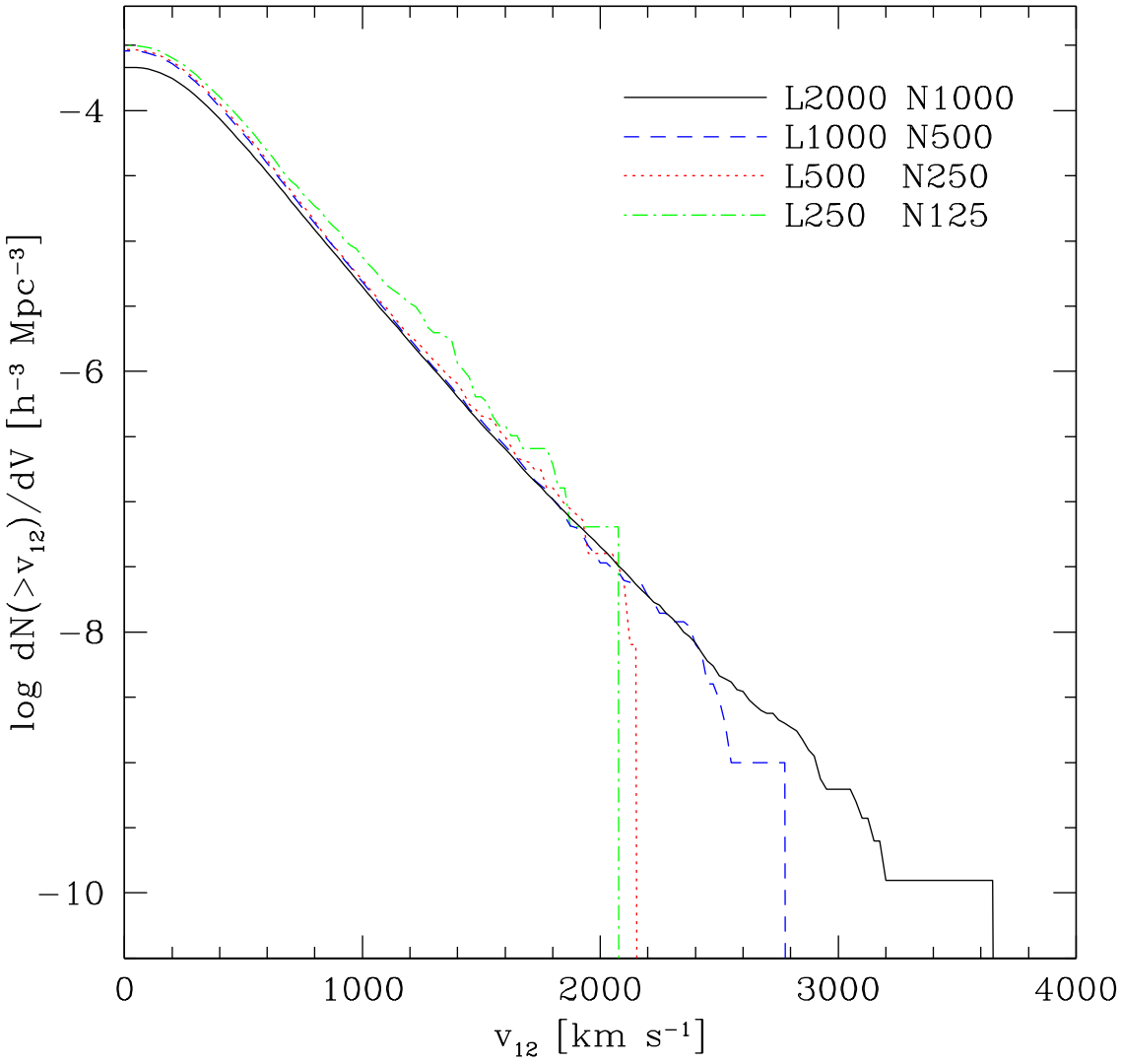

Figure 9 DM halo cumulative velocity function, box size effect. Increasing the box size increases the number of high velocity pairs we find. The trend seems to be present throughout all simulations presented in this figure.

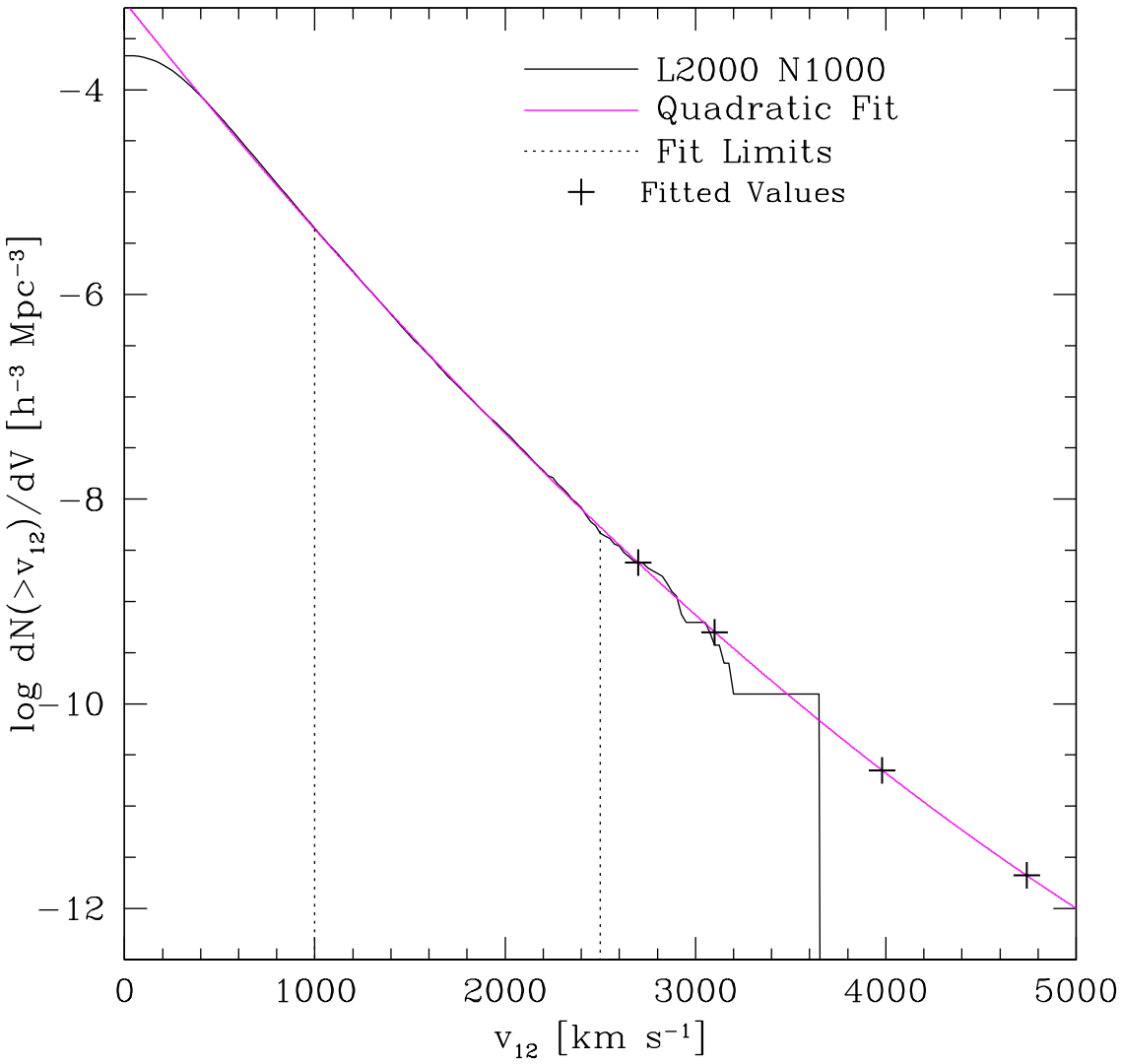

Figure 10 Quadratic fit between the velocities of 1000 and 2500 applied to the L2000N1000 z=0 cumulative velocity curve. If the trend continues as we enlarge the simulation box, we expect to find one halo pair with pairwise velocities of 4740, 3980, 3100, & 2700 km s^{-1} within a box size of $\simeq$ 3612, 2657, 1689, 1315 h^{-1} Mpc respectively.

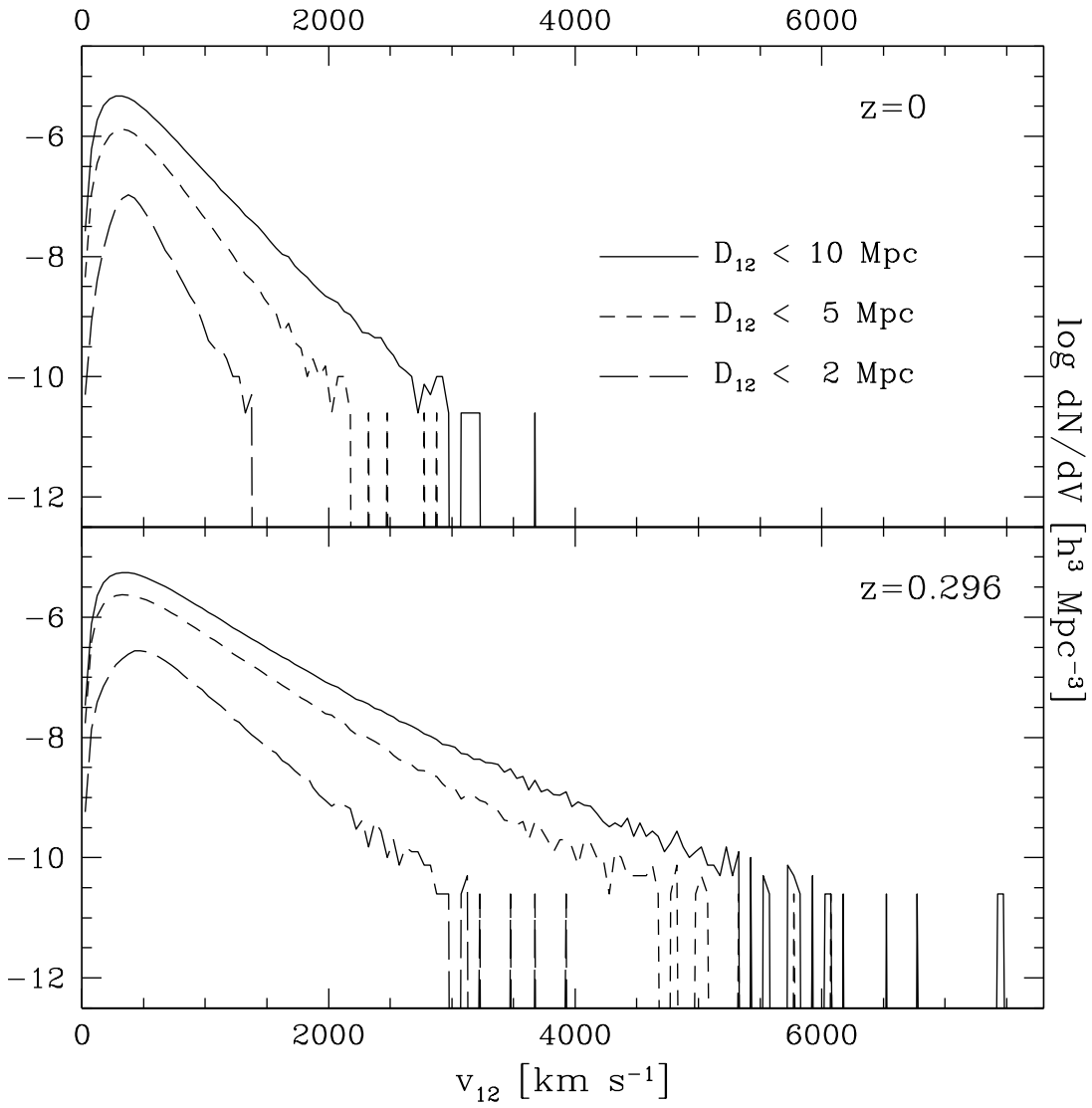

Figure 11 Top Panel: Reproduction of the bottom panel of Figure 4. Bottom Panel: L2000N1000 velocity function at a redshift of z=0.296 showing that as we go to larger redshifts the pairwise velocities of all halos increase.

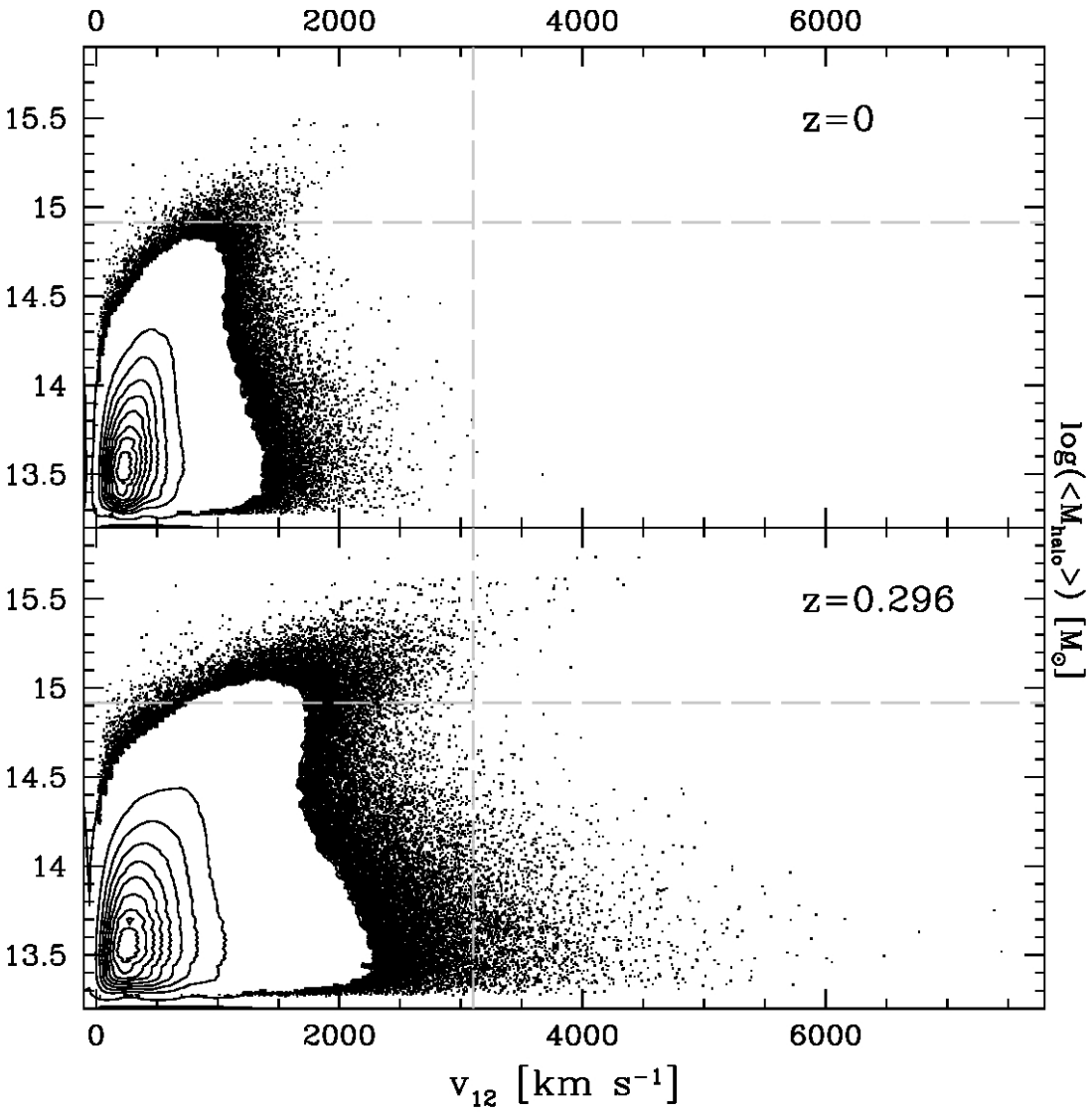

Figure 12 Top Panel: Reproduction of the bottom panel in Figure 6. Bottom Panel: L2000N1000 velocity vs. mass plot at a redshift of z=0.296 showing that as we go to larger redshifts the pairwise velocities of larger mass halos increase. The vertical dashed line represents v_{12}=3100 km s^{-1}, and the horizontal dashed line represents the average mass of 1E0657-56.

REFERENCES

Blumenthal, G. et al. 1984, Nature, 311, 517

Bradač, M. et al. 2006, ApJ, 652, 937

Clowe, D. et al. 2004, ApJ, 604, 596

—. 2006, ApJ, 648, L109

Crocce, M. et al. 2010, , in press, arXiv:0907.0019

Davis, M. et al. 1985, ApJ, 292, 371

Friedmann, A. 1922, Zeitschrift für Physik A Hadrons and Nuclei, 10, 377

—. 1924, Zeitschrift für Physik A Hadrons and Nuclei, 21, 326

Komatsu, E. et al. 2009, ApJ, 180, 330

—. 2010, ApJ, in press, arXiv:1001.4538

Kowalski, M. et al. 2008, ApJ, 686, 749

Lee, J. & Komatsu, E. 2010, ApJ, in press, arXiv:1003.0939

Lemaître, G. 1927, Annales de la Société Scientifique de Bruxelles, 47, 49

Markevitch, M. 2006, ESA, SP-604, 723

Mastropietro, C. & Burkert, A. 2008, , 389, 967

Milosavljević, M. et al. 2007, ApJ, 661, L131

Mo, H. & White, S. 2002, , 336, 112

Ostriker, J. & Peebles, P. 1973, ApJ, 186, 467

Robertson, H. 1935, ApJ, 82, 248

—. 1936a, ApJ, 83, 187

—. 1936b, ApJ, 83, 257

Rubin, V. et al. 1980, ApJ, 238, 471

Springel, V. 2005, , 364, 1105

Springel, V. & Farrar, G. 2007, AS, 380, 911

Springel, V. et al. 2001, , 328, 726

Walker, A. 1937, Proceedings of the London Mathematical Society, s2-42(1), 90

Wright, E. 2006, PASP, 118, 1711

Zwicky, F. 1937, ApJ, 86, 217

VITA

Graduate College
University of Nevada, Las Vegas

Robert Jo Thompson

Degrees:

Associate of Science, 2004
Community College of Southern Nevada

Bachelor of Sciences, Physics, 2008
University of Nevada Las Vegas

Thesis Title: Velocity Distribution of Dark Matter Halos: a Critical Test for the Λ Cold Dark Matter Model

Thesis Examination Committee:

Chairperson, Kentaro Nagamine, Ph. D.
Committee Member, Daniel Proga, Ph. D.
Committee Member, George Rhee, Ph. D.
Graduate Faculty Representative, Balakrishnan Naduvalath, Ph. D.